



Synthesis, characterization and performance of iron oxide/alumina-based nano-adsorbents for simultaneous arsenic and fluoride removal

T.C. Prathna^{a,*}, Dian Novita Sitompul^a, Saroj Kumar Sharma^a, Maria Kennedy^{a,b}

^a*Environmental Engineering and Water Technology Department, IHE Delft Institute for Water Education, 2601 DA, Delft, The Netherlands, emails: prathna.tc@gmail.com (T.C. Prathna), dianheartuser@gmail.com (D.N. Sitompul), s.sharma@un-ihe.org (S.K. Sharma), m.kennedy@un-ihe.org (M. Kennedy)*

^b*Faculty of Civil Engineering, Delft University of Technology, Stevinweg 1, 2628 CN, Delft, The Netherlands*

Received 22 October 2017; Accepted 15 January 2018

ABSTRACT

The study was designed to synthesize iron oxide/alumina nanocomposites and to investigate their application as an adsorbent to remove both fluoride and arsenic from aqueous solutions. The nanocomposites were extensively characterized by X-ray diffraction analysis, Brunauer–Emmett–Teller analysis, Fourier transform infrared spectroscopy and zeta potential analysis. The size and morphology of the particles were determined by scanning electron microscopy which revealed an average particle size of ~230 nm. The synthesized nanocomposites were stable for at least 4 h in static conditions as evidenced by particle size measurements. Batch sorption studies were carried out and sorption isotherms and reaction kinetics were analyzed. The nanocomposites followed the Langmuir isotherm model and fitted well with pseudo-second-order reaction for both As and F. The maximum sorption capacity of the nanocomposites for As(III), As(V) and F at pH 7 was 1,136 µg/g, 2,513 µg/g and 4 mg/g, respectively. The presence of F in the model water had a synergistic effect on As(III) and As(V) removal whereas the presence of As had no significant effect on F removal at pH 7. Furthermore, the nanocomposites demonstrated significant antibacterial activity at a concentration of 4 mg/mL with ~3 log reduction of *Escherichia coli* after 24 h. The results of the study showed that the synthesized nanocomposites can be a promising adsorbents for As and F removal in small-scale water systems.

Keywords: Iron oxide; Alumina; Nanocomposites; Adsorption; Arsenic; Fluoride

1. Introduction

Pollution and indiscriminate exploitation of surface water over the years has led to dependence on groundwater for potable purposes by over 50% of the global population [1]. However, groundwater is a source of several naturally occurring and anthropogenic ions such as fluoride, arsenic, lead, chromium, nitrate, selenium, chloride, heavy metals, radioactive materials in addition to pathogens which greatly compromise the water quality [2,3]. The World Health Organization reports that about 663 million people around the world do not have access to safe drinking water [4].

Furthermore, drinking water contamination with microbial pathogens causes several waterborne diseases [5,6]. Globally, lack of safe drinking water and adequate sanitation lead to 842,000 deaths per year, mostly due to diseases caused by bacteria, viruses, protozoa and parasites [7]. Hence, implementation of basic water treatment is urgently needed, particularly in vulnerable areas, where centralized water treatment facilities are non-existent [8].

Arsenic and fluoride are reported among the most hazardous inorganic pollutants present in groundwater [9]. In view of their adverse health impact, WHO has recommended maximum permissible limits of F and As as 1.5 mg/L and 10 µg/L, respectively [10]. Co-contamination of arsenic and fluoride in groundwater has been reported in many parts

* Corresponding author.

of the world [11,12]. Hence, simultaneous removal of both arsenic and fluoride is of crucial importance to simplify treatment processes and to reduce costs [13].

Technologies such as reverse osmosis and ion exchange are effective in simultaneously removing arsenic and fluoride in centralized water treatment facilities but are however restricted in their application due to the high costs of implementation [13]. On the other hand, adsorption technology is preferred in small-scale systems in view of its cost-effectiveness and high efficiency [14]. Iron-based adsorbents have been extensively reported to exhibit the highest adsorption capability towards As while aluminium-based adsorbents have been shown to have affinity towards F [15,16].

Few studies have been carried out exploring the efficacy of iron- and aluminium-based binary oxides and hydroxides for the simultaneous removal of As and F [12,13]. Recent decades have witnessed an increasing interest in the application of nanoparticles in drinking water treatment in view of their increased surface area to volume ratio [17] enabling enhanced adsorption of contaminants. Our previous study had explored the potential of iron-based nanoadsorbents for the removal of arsenic and fluoride [16]. However, the nanoparticles exhibited significant activity towards arsenic, their efficacy for fluoride removal was not comparable with aluminium-based adsorbents. Some studies have also indicated the potential antimicrobial activity of alumina and iron oxide nanoparticles against common pathogens [18,19].

Thus, the objectives of the present study were to elucidate the simultaneous arsenic and fluoride removal potential of iron oxide/alumina nanocomposites. In order to achieve this, iron oxide/alumina nanocomposites were synthesized, characterized and their simultaneous arsenic and fluoride removal efficiency were studied. Additionally, as a secondary study, their antibacterial efficacy towards *Escherichia coli*, a common pathogen, was extensively studied.

2. Materials and methods

2.1. Chemicals

Iron(III) chloride hexahydrate, iron(II) chloride tetrahydrate and aluminium(III) nitrate nonahydrate were procured from Merck KGaA, Germany. NaF was used to prepare standard fluoride solutions while NaAsO₂ and NaAsO₄·12H₂O were used as sources of As(III) and As(V), respectively. All chemicals were of analytical grade and were used without further purification. Deionized water from Milli-Q was used throughout the experiments.

2.2. Synthesis of iron oxide/alumina nanocomposites

2.2.1. Preparation of iron oxide (Fe₃O₄) nanoparticles

The magnetic nanoparticles were prepared by a chemical coprecipitation method as reported in our previous publication [16]. Briefly, 0.279 g of FeCl₃·6H₂O and 1.395 g of FeCl₂·4H₂O were dissolved in 100 mL ethanol and 14.7 M NH₃ was added dropwise while stirring until pH reached 9. Agitation was further continued at 50°C for 3 h and the contents centrifuged. The pellet was further washed and dried at 100°C for 3 h.

2.2.2. Preparation of iron oxide/alumina nanocomposites

The method of Amirjalali and Shayesteh [20] was followed with modifications. 3.75 g Al(NO₃)₃·9H₂O was dissolved in 100 mL deionized water and heated to 60°C with stirring. It was then precipitated by adding NH₃ (2 M) at the rate of 2 mL/min thereby forming Al(OH)₃ gel. 0.05 g of the synthesized iron oxide nanoparticles were added followed by stirring at room temperature for 12 h. The contents were centrifuged at 4,500 rpm for 10 min and repeatedly washed. The pellet was then dried at 100°C for 1 h followed by calcination at 550°C for 3 h.

2.3. Physicochemical characterization

2.3.1. X-ray diffraction analysis

Preliminary characterization of the nanocomposites was performed using an XRD diffractometer (PANalytical-XPRT PRO diffractometer system, Eindhoven, Netherlands). The target was Cu K α with a wavelength of 1.54060 Å. The generator was operated at 40 kV and with a 30 mA current. The scanning range was selected between 10° and 100°.

2.3.2. Brunauer–Emmett–Teller analysis

The specific surface area of the synthesized nanocomposites was determined using Brunauer–Emmett–Teller (BET) surface area analyzer (Micromeritics TriStar III, USA). The samples were placed in sample cells degassed, and heated to 300°C for 2 h and cooled down to room temperature to remove moisture prior to analysis. The adsorption–desorption plots were used to calculate the specific surface area (N₂/BET method).

2.3.3. Fourier transform infrared spectroscopic analysis

The surface functional groups of the nanocomposites were determined using a FTIR spectrophotometer (Affinity-1 FTIR spectrometer, Shimadzu, Japan) over the range 500–4,000 cm⁻¹.

2.3.4. Particle size analysis

The particle size range of the nanocomposites along with its polydispersity was determined using a particle size analyzer (Zetasizer Nano ZS, Malvern Instruments Ltd., UK). The particles were dispersed in deionized water prior to analysis.

2.3.5. Zeta potential analysis

The surface electrostatic potential of the nanocomposites was determined using a zeta potential analyzer (Zetasizer Nano ZS, Malvern Instruments Ltd., UK). The particles were dispersed in 10⁻³ M KCl as a background electrolyte prior to measurement. Measurement was performed at various pH to determine the point of zero charge (PZC) of the particles.

2.3.6. Scanning electron microscopy–energy dispersive analysis X-ray spectroscopy

The surface morphology of the particles was determined using SEM (JSM-6010LA, JEOL Inc., USA) and the particles

were dispersed in deionized water. The dispersed particles were then directly coated onto carbon tape and air dried prior to analysis. The elemental composition of the nanocomposites was determined using scanning electron microscopy–energy dispersive analysis X-ray spectroscopy (SEM–EDAX).

2.3.7. Particle stability

The stability of the synthesized particles over time was determined by measuring the difference in particle size. The solution containing nanocomposites was left undisturbed and sampling was done at different time points using a particle size analyzer.

2.4. Batch adsorption studies

2.4.1. Effect of initial concentration

Effect of As(III) and As(V) on adsorption by iron oxide/alumina nanocomposites was determined by adding 0.05 g of nanoparticles in 50 mL of different concentrations of arsenic namely 200, 500, 1,000, 1,500 and 2,000 µg/L As(III) and As(V), respectively. Studies were carried out at pH 7. The bottles were kept agitated at 180 rpm (Innova 2100 Platform Shaker, New Brunswick Scientific, USA) for 4 h at room temperature (20°C). Similarly, the effect of fluoride was studied at different concentrations of fluoride namely 1, 3, 5, 7 and 10 mg/L F.

2.4.2. Effect of adsorbent dosage

Effect of adsorbent dosage on As and F removal was studied for different weights of nanocomposites namely 0.5, 1 and 2 g/L. Studies were carried out at pH 7 and at fixed initial concentration of 500 µg/L As and 3 mg/L F, respectively.

2.4.3. Effect of coexistence of As and F

Effect of coexistence of F on As adsorption was determined by adding 0.05 g of nanocomposites in 50 mL of arsenic at initial concentrations of 200, 500, 1,000, 1,500 and 2,000 µg/L in the presence of fixed concentration of F (3 mg/L). Similarly, effect of coexistence of As on F adsorption was determined at different initial concentration of F, namely, 3, 5, 7 and 10 mg/L in the presence of fixed concentration of As(III) and As(V) (500 µg/L).

2.5. Adsorption isotherms

Adsorption isotherms were obtained by batch equilibration technique carried out for a time period of 4 h. Isotherm experiments were performed at different pH values namely 6.5, 7 and 7.5 with varying concentrations of As(III), As(V) and F as mentioned in the previous section. Langmuir and Freundlich isotherms were used to fit the adsorption data from equilibrium experiments.

2.6. Adsorption kinetics

The sorption capacity and percentage sorption of both As(III) and As(V) and F as a function of time were determined by performing a study until equilibration time (15 min to 4 h). The concentration of As(III) and As(V) selected for

the study was 500 µg/L at pH 7. The data obtained were then plotted to determine the best fitting kinetic model. All the experiments were performed in triplicates.

2.7. Chemical analysis

2.7.1. Arsenic

Samples were withdrawn at specific points in time and filtered through a 0.45 µm filter. Post-filtration, the samples were diluted and acidified with concentrated nitric acid before analyzed using an atomic absorption spectrophotometer-graphite furnace (Solar Thermo Elemental with FS95 graphite furnace with autosampler) with a detection limit of 2 µg/L.

2.7.2. Fluoride

The filtered samples withdrawn at specific points in time were added in equal volume to TISAB III buffer (to release any complexed fluoride ions) before measurement using a fluoride ion selective electrode (WTW F 800 DIN, Germany).

The adsorption capacity was estimated by Eq. (1) as follows:

$$q_e = \frac{(C_o - C_e)V}{m} \quad (1)$$

The adsorption (%) was determined using the following equation:

$$\text{Adsorption (\%)} = \frac{(C_o - C_e)}{C_o} \times 100 \quad (2)$$

where q_e is the adsorption capacity (mg/g), C_o and C_e are the initial and equilibrium concentration (µg/L and mg/L for As(III), As(V) and F, respectively) of the contaminant, respectively, V is the volume of As and F solution (L) and m is the mass of the iron oxide/alumina nanocomposites.

2.8. Antibacterial activity of the nanocomposites

The antibacterial activity of the nanocomposites was tested against *E. coli* (ATCC 25922).

2.8.1. Growth inhibitory effect based on growth curve method

1 mL of fresh *E. coli* culture containing 10^9 CFU/mL was transferred to Erlenmeyer flasks containing 50 mL of nutrient broth. Different concentrations of the nanocomposites, namely, 1, 2 and 4 mg/mL were added to the flasks containing the culture. The flasks were maintained at 37°C for 24 h at 180 rpm and the absorbance was measured at 600 nm using a spectrophotometer (Cecil 1100, Cecil Instruments, UK) at different time points [21].

2.8.2. Growth inhibitory effect based on plate count method

Overnight cultures of *E. coli* (10^9 CFU/mL) were diluted using 0.85% peptone physiological salt (PPS) solution to a final

concentration of 10^4 CFU/mL. 1 mL from this diluted culture was then added to 9 mL of PPS containing different concentrations of nanocomposites, namely, 1, 2 and 4 mg/mL. The tubes were then maintained at 37°C for 24 h at 180 rpm. Samples of 100 μL each were taken at 0, 2, 4, 8 and 24 h and plated on Chromocult coliform agar (CCA) plates and incubated at 37°C and counted for viable bacteria [21]. *E. coli* colonies are stained dark pink in the CCA plates. The antibacterial rate (%) [22] was calculated using the following equation:

$$\text{Antibacterial rate} = 1 - \frac{\text{CFU}_{\text{test}}}{\text{CFU}_{\text{control}}} \times 100 \quad (3)$$

The log removal of *E. coli* at different time intervals was also calculated.

3. Results and discussion

3.1. Synthesis of iron oxide/alumina nanocomposites

The synthesis of the nanocomposites was carried out in two steps. The first step involved the synthesis of iron oxide nanoparticles using a chemical coprecipitation method. Spherical nanoparticles of ~ 190 nm were obtained. More details on its characteristics can be found in Prathna et al. [16]. The next step involved the synthesis of the nanocomposites. Addition of ammonia solution to the aluminium nitrate solution resulted in the formation of aluminium hydroxide. Further addition of iron oxide nanoparticles at this stage resulted in the change in colour of the white opaque solution to pale red. Further calcination of the contents resulted in the conversion of hydroxides to oxide and was used for further characterization studies.

3.2. Physicochemical characterization

3.2.1. XRD analysis

The X-ray diffraction (XRD) pattern of the nanocomposites (Fig. 1) revealed that iron oxide existed in the adsorbent. The peaks at 35° and 57° could be assigned to the characteristic

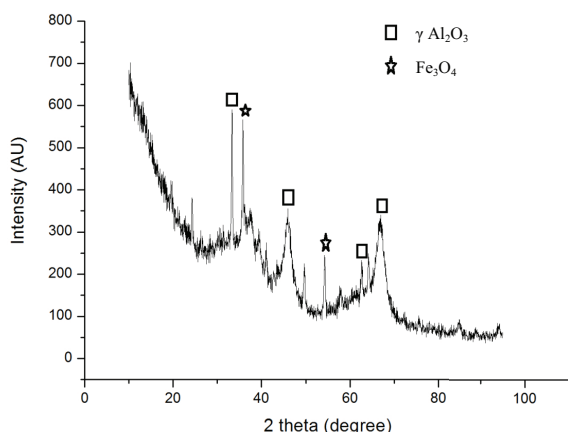


Fig. 1. XRD pattern of synthesized iron oxide/alumina nanocomposites.

peaks of Fe_3O_4 representing (311) and (511) facets [23]. Peaks at 32° , 46° , 62° and 68° could be assigned to (220), (400), (511) and (440) facets of Al_2O_3 (JCPDS File No. 29-0063) implying that it was predominantly $\gamma\text{-Al}_2\text{O}_3$ [24]. Previous studies on γ -alumina nanoparticles prepared by a similar method [20] showed peaks corresponding to the same planes as shown in Fig. 1. XRD analysis confirmed the crystallinity of the nanocomposites.

3.2.2. BET analysis

BET method was employed to measure the specific surface area of the iron oxide/alumina nanocomposites. A slight increase in the surface area of nanocomposites (86.08 ± 1.08 m^2/g) was observed as compared with the iron oxide nanoparticles (75.24 m^2/g) [16]. Increase in the surface area of the nanocomposites was possibly due to the decoration of pristine iron oxide nanoparticles in the composites [25] and may play a role in enhanced adsorption applications [26]. Related studies on the specific surface area of sulphate-doped $\text{Fe}_3\text{O}_4/\text{Al}_2\text{O}_3$ nanoparticles yielded a surface area of 63.37 m^2/g [23].

3.2.3. FTIR analysis

Fourier transform infrared (FTIR) analysis was performed to determine the functional groups present in the synthesized nanoadsorbent. Fig. 2 shows the presence of absorption bands at $\sim 3,500$ and $\sim 3,720$ cm^{-1} which could be assigned due to $-\text{OH}$ stretch [27]. The strong peak at $\sim 2,360$ cm^{-1} can be assigned to $-\text{C}-\text{O}$ bend while the peak at $\sim 2,063$ cm^{-1} corresponds to symmetric deformation vibrations of $\text{Al}-\text{OH}$ [28]. The band at $\sim 1,680$ cm^{-1} was due to $\text{H}-\text{O}-\text{H}$ scissoring mode [20] and the small peak at ~ 640 cm^{-1} could be related to $\text{Fe}-\text{O}$ bond vibration of Fe_3O_4 nanoparticles in the sample [29]. The peak at $\sim 1,540$ cm^{-1} could be attributed to the interaction between Fe oxide and Al oxide within the nanocomposites [13]. XRD and FTIR analyses confirmed the presence of Al and Fe in the adsorbent.

3.2.4. Particle size analysis

Particles of around 236 ± 3 nm in diameter were observed as seen from particle size analysis studies. The particles had

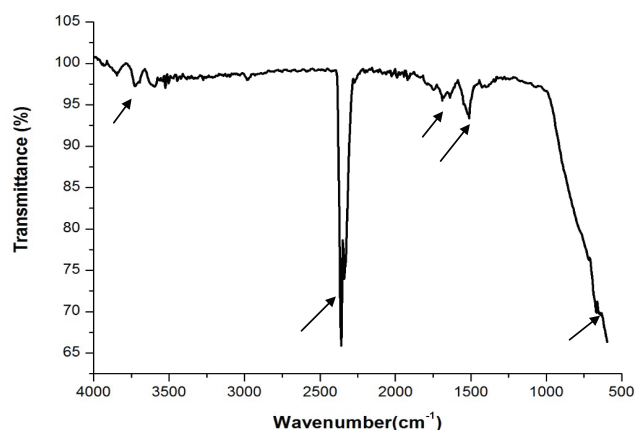


Fig. 2. FTIR spectroscopy of iron oxide/alumina nanocomposites.

a narrow size range with a polydispersity of 0.338. Thus, the particle size analysis revealed the synthesis of nearly mono-disperse particles with low polydispersity.

3.2.5. Zeta potential analysis

The zeta potential of the iron oxide/alumina nanocomposites was measured at varied pH and the PZC was observed at pH ~6.8. A decrease in surface zeta potential was observed with a corresponding increase in pH. The surface zeta potential was 43.03 ± 1.91 mV at pH 2 and it decreased to -30.4 ± 0.64 mV at pH 10 (Fig. 3). The PZC of iron oxide nanoparticles added during the synthesis was pH ~9 [16]. Das et al. [30] observed the PZC of alumina nanoparticles to be pH ~6.7 depending on the method of synthesis.

3.2.6. SEM–EDAX studies

Fig. 4(a) shows the SEM image of the nanocomposites dispersed in aqueous solution. Nearly spherical particles with aggregates were observed from the image. EDAX analysis confirmed the presence of iron (Fe) and aluminium (Al) in the samples (Fig. 4(b)).

3.2.7. Stability of nanocomposites

The stability of the nanocomposites was also studied by measuring the change in particle size over a period of 4 h under static conditions. The results of the study are shown in Fig. 5. There was no significant change in particle size over a period of 4 h. At the end of 4 h, the particle size decreased by ~20 nm signifying the settling of larger particles under static conditions.

3.3. Batch adsorption studies

Batch adsorption studies were carried out to study the effect of various parameters such as initial concentration of arsenic and fluoride, adsorbent dosage and pH.

3.3.1. Effect of initial concentration

3.3.1.1. Arsenic The effect of As initial concentration on the adsorption efficiency of iron oxide/alumina nanocomposites was investigated in the present study. Figs. 6(a) and (b) show the adsorption efficiency (%) and adsorption capacity (q_e) of iron oxide/alumina nanocomposites as a function of As(III) and As(V) initial concentration, respectively. In both cases, the adsorption capacity (q_e) was observed to increase with a corresponding increase in the As(III) and As(V) concentrations, respectively (at the concentrations studied). Similar trend will be observed as long as the nanocomposites are not saturated with the adsorbed species (namely As and F). From the figures, it was observed that q_e was higher for As(V) compared with As(III). At 1,000 $\mu\text{g/L}$ initial concentration of As(III) and As(V), the adsorption capacity of the nanocomposites, q_e was 568 and 878 $\mu\text{g/g}$, respectively (Figs. 6(a) and (b)). Iron-based materials have been extensively studied for arsenic removal in view of their strong adsorption specificity towards arsenic and also their ease of removal exploiting their magnetic properties [31]. The removal of arsenate and arsenite by Fe-based materials occurs due to As–Fe complexation

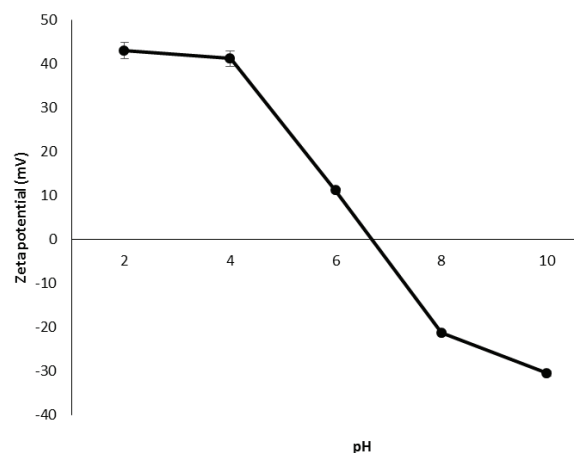


Fig. 3. Change in zeta potential of iron oxide/alumina nanocomposites vs. pH.

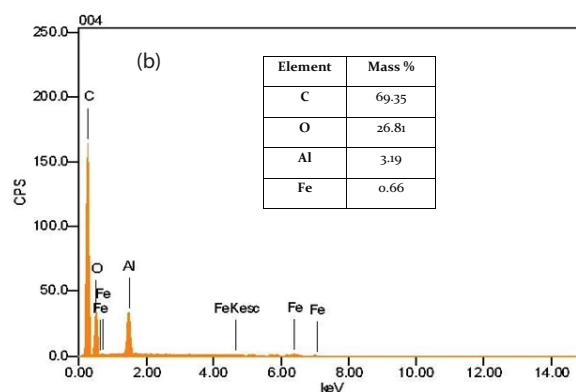
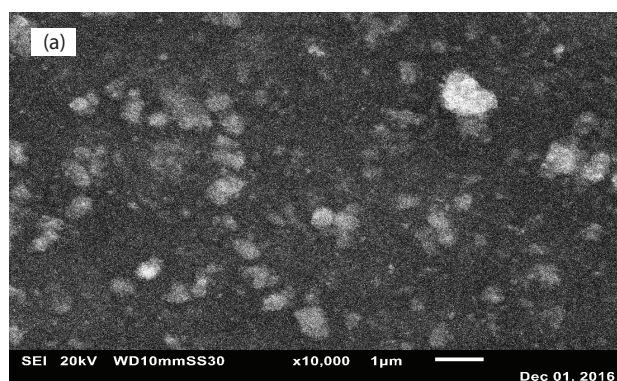


Fig. 4. (a) SEM micrograph and (b) EDAX analysis of iron oxide/alumina nanocomposites.

occurring on its surface [32]. As(V) predominates in aerobic environments while As(III) is predominantly found in moderately reducing anaerobic environments [33]. Studies have indicated that the mobility and toxicity of As(III) is greater than As(V) [34] and therefore it is essential to develop an adsorbent which is also effective against As(III). Our previous studies with iron oxide nanoparticles indicated an adsorption capacity, q_e , of 954 $\mu\text{g/g}$ at 1,000 $\mu\text{g/L}$ initial concentration of As(III) [16].

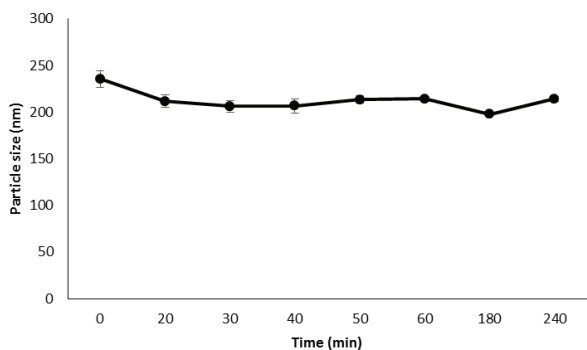


Fig. 5. Stability study of synthesized iron oxide/alumina nanocomposites.

3.3.1.2. *Fluoride* Fig. 6(c) shows the effect of initial F concentration on adsorption efficiency (%) and adsorption capacity (mg/g) of the iron oxide/alumina nanocomposites. Increase in the initial F concentration led to a corresponding increase in the adsorption capacity, q_e , of iron oxide/alumina nanocomposites. At 10 mg/L initial concentration of F, the adsorption capacity of the nanocomposites was 3.60 mg/g. The amount of F adsorbed at pH 7 (3.60 mg/g) was approximately two times higher as compared with our previous study carried out using iron oxide nanoparticles (1.78 mg/g) [16]. A decrease in the percentage removal of fluoride was also observed with increase in the initial concentration and this could possibly be due to limited active sites on the adsorbent [35].

3.3.2. Effect of adsorbent dosage

The influence of adsorbent dose on percentage of As(III), As(V) and F removal at an initial As concentration of 500 $\mu\text{g/L}$ and F concentration of 3 mg/L, respectively, at a neutral pH is shown in Table 1. In all cases, it could be observed that increase in the adsorbent dose from 0.5 to 2 g/L led to an increase in the percentage removal of As and F. In case of F, it was apparent that increase in the adsorbent dose from 0.5 to 1 g/L led to nearly a twofold increase in the percentage removal. This could be attributed to the increasing active site/F ratio with increase in adsorbent dose [31]. However, further increase in adsorbent did not lead to significant increase in the percentage removal. Increase in adsorbent dose did not significantly impact the As(V) removal and on an average, ~98%–99% removal of As was achieved. Therefore, for further studies an adsorbent dose of 1 g/L was used.

3.4. Isotherm studies

3.4.1. Effect of pH

Solution pH plays a major role in determining the behaviour on an adsorbent [36]. In order to further determine the mode of adsorption of the nanocomposites, isotherm studies were carried out at different pH (pH 6.5, 7 and 7.5) and the data analyzed. Langmuir and Freundlich isotherm models were fitted to the experimental data to determine the maximum adsorption capacity of iron oxide/alumina nanocomposites towards As(III), As(V) and F [37].

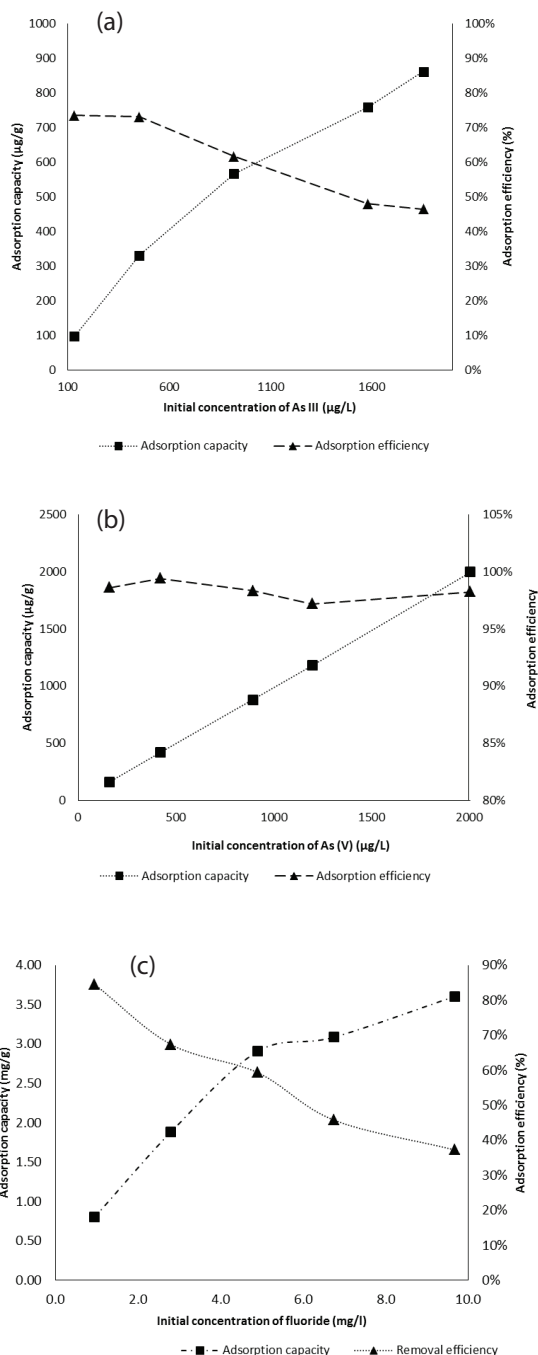


Fig. 6. Adsorption capacity and percentage adsorption of iron oxide/alumina nanocomposites as a function of (a) As(III), (b) As(V) and (c) F concentration (pH = 7.0, shaking speed = 180 rpm, temperature = 20°C).

The Langmuir isotherm model assumes that adsorption takes place by monolayer sorption without involving intermolecular forces and also assumes that the adsorbent surface is homogenous [38]:

$$\frac{C_e}{q_e} = \frac{1}{q_m} C_e + \frac{1}{k_x q_m} \quad (4)$$

Table 1

Effect of adsorbent dose on percentage arsenic and fluoride removal by iron oxide/alumina nanocomposites (pH = 7; shaking speed = 180 rpm; temperature = 20°C)

Weight of adsorbent (g/L)	Percentage removal		
	As(III)	As(V)	F
0.5	53.4	98.9	32.7
1	64.2	98.4	61.9
2	67.1	99.9	74.5

while the Freundlich model is an empirical description of adsorption on a heterogeneous surface [39].

$$\log q_e = \log k_f + \frac{1}{n} \log C_e \quad (5)$$

where q_e is the amount of sorbate adsorbed at equilibrium per gram of iron oxide/alumina nanocomposites; C_e is the concentration of sorbate at equilibrium; q_m is monolayer sorption capacity (mg/g); k_a is the Langmuir sorption equilibrium constant and k_f and $1/n$ are the Freundlich constants.

3.4.1.1. Arsenic pH is a major factor for arsenic adsorption-based water treatment processes as arsenic speciation is strongly influenced by the water pH value [40]. In case of As(III) and As(V), the Langmuir equilibrium isotherm equation gave relatively better description of sorption. Fig. 7(a) plots the Langmuir isotherm for As(III) adsorption. It could be observed that increase in pH from 6.5 to 7.5, did not lead to a significant change in the q_m value (slight increase from 1,064 to 1,333 $\mu\text{g/g}$, respectively). This might be due to the dominant As(III) species as neutral H_3AsO_3 at the pH range studied [41]. However, in case of As(V) (Fig. 7(b)), it could be observed that increase in pH from 6.5 to 7.5 led to a significant decrease in the q_m value from 2,857 to 1,923 $\mu\text{g/g}$, respectively (Table 2). It is well known that As(V) predominantly exists as negatively charged H_2AsO_4^- and HAsO_4^{2-} in the pH range studied [42]. Since the PZC of the nanocomposites was observed to be pH ~ 6.8 (Fig. 3), they were slightly positively charged at pH lower than 6.8 favouring the adsorption of arsenic(V) anions due to electrostatic attraction. Further increase in pH possibly led to repulsion effect. Similar experimental phenomenon was also observed for the adsorption of As(III) and As(V) by magnetic nanoparticles impregnated chitosan beads [31]. Comparing the q_m values between As(III) and As(V) showed that iron oxide/alumina nanocomposites had ~ 3 times more adsorption capacity for As(V) than As(III) at pH 6.5, suggesting that the nanocomposites had higher sorption capacity for As(V) than As(III).

3.4.1.2. Fluoride Data analysis for F adsorption demonstrated a good fit with both Langmuir and Freundlich isotherms. Fig. 7(c) plots the Langmuir isotherm for F adsorption. There was no effect on the q_m values with increase in pH in the range studied. A maximum q_m value of 4.2 mg/g was observed at pH 6.5 and this was ~ 2.5 times

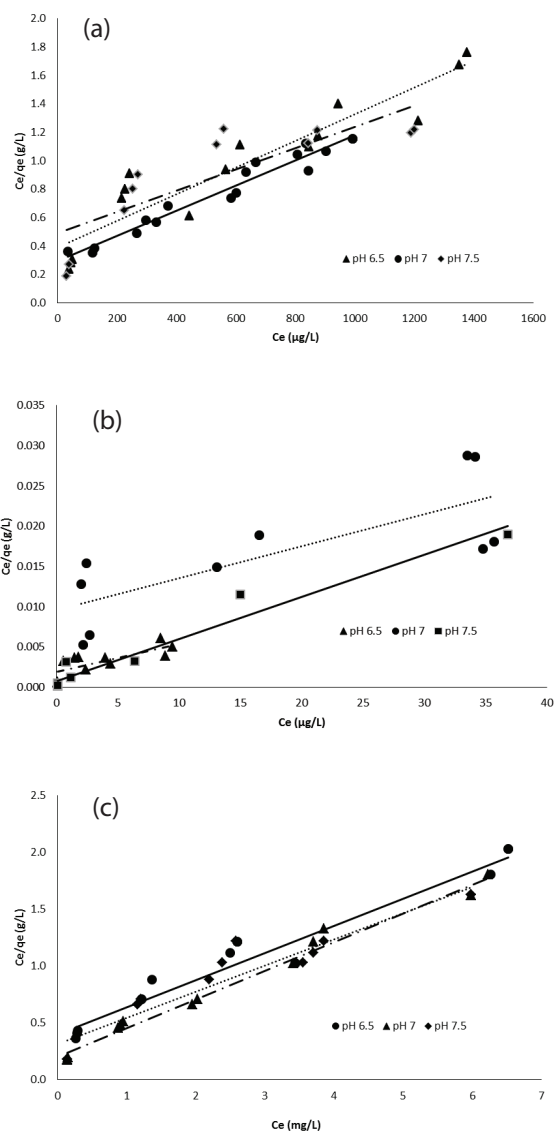


Fig. 7. Langmuir isotherm of (a) As(III), (b) As(V) and (c) F adsorption onto iron oxide/alumina nanocomposites.

higher than the q_m values observed using iron oxide nanoparticles in our previous research [16]. Kamga et al. [43] reported that the q_m values of fluoride onto boehmite nanoparticles synthesized using NH_4Cl to be 10.25 mg/g. However, the study was carried out at a higher initial fluoride concentration and at a higher adsorbent dose (4 g/L) and agitation time (24 h). Similarly, Kumar et al. [14] explored the potential of Al-Fe doped nanopolymeric adsorbents for the removal of fluoride and arsenic(V) from wastewater and reported a maximum adsorption capacity of ~ 100 mg/g for fluoride (under higher initial fluoride concentration ranging between 10 and 100 mg/L).

It was significant to observe from the isotherm studies that the q_m values for As did not change significantly as compared with iron oxide nanoparticles. On the other hand, there was a significant increase in the q_m values for F as compared with the nanoparticles. This further signified that iron

oxide/alumina nanocomposites could potentially be used for the removal of both arsenic and fluoride at drinking water pH range.

3.4.2. Effect of coexisting arsenic and fluoride

Coexistence of arsenic and fluoride has been reported in many aquifers and hence there is a need to develop technologies to simultaneously remove the coexisting As and F from

Table 2
Summary of parameters obtained from Langmuir isotherms for arsenic and fluoride adsorption by iron oxide/alumina nanocomposites

Contaminant	Langmuir model	
	q_m ($\mu\text{g/g}$)	R^2
As(III) + F	2,222.0	0.84
As(III)	1,136.0	0.96
As(V) + F	2,857.0	0.71
As(V)	2,513.0	0.61
F + As(III)	3.85	0.95
F	4.00	0.98

groundwater. Though there have been studies on the application of nanoadsorbents for simultaneous removal of As and F, very few of them have explored the removal of either As or F in the presence of the other [12]. A system containing a mixture of ions/adsorbates are known to exhibit three different types of behaviour, namely (i) synergism (the effect of the mixture is greater than the individual components), (ii) antagonism (the effect of the mixture is lesser than the individual components) and (iii) non-interaction [35].

3.4.2.1. Arsenic adsorption in the presence of fluoride Fig. 8(a) plots the Langmuir isotherm for As(III) in the presence of fluoride and Table 2 provides a summary of parameters. It could be observed that the presence of F provided a synergistic effect and led to an increase in the q_m values from 1,136 to 2,222 $\mu\text{g/g}$ in the absence and presence of fluoride, respectively. Similarly the presence of fluoride led to a slight increase in the As(V) removal capacity (q_m values increased from 2,513 to 2,857 $\mu\text{g/g}$ in the presence of fluoride) and the data fitted Langmuir isotherm model (Fig. 8(b)) indicating that the negatively charged arsenate ions competed effectively for the active sites on the adsorbent than the negatively charged fluoride ion [12]. Similar results were reported by Rathore et al. [35] when they studied the removal of arsenic by chemically treated laterite in the presence of fluoride. On the other hand, Qiao et al. [12]

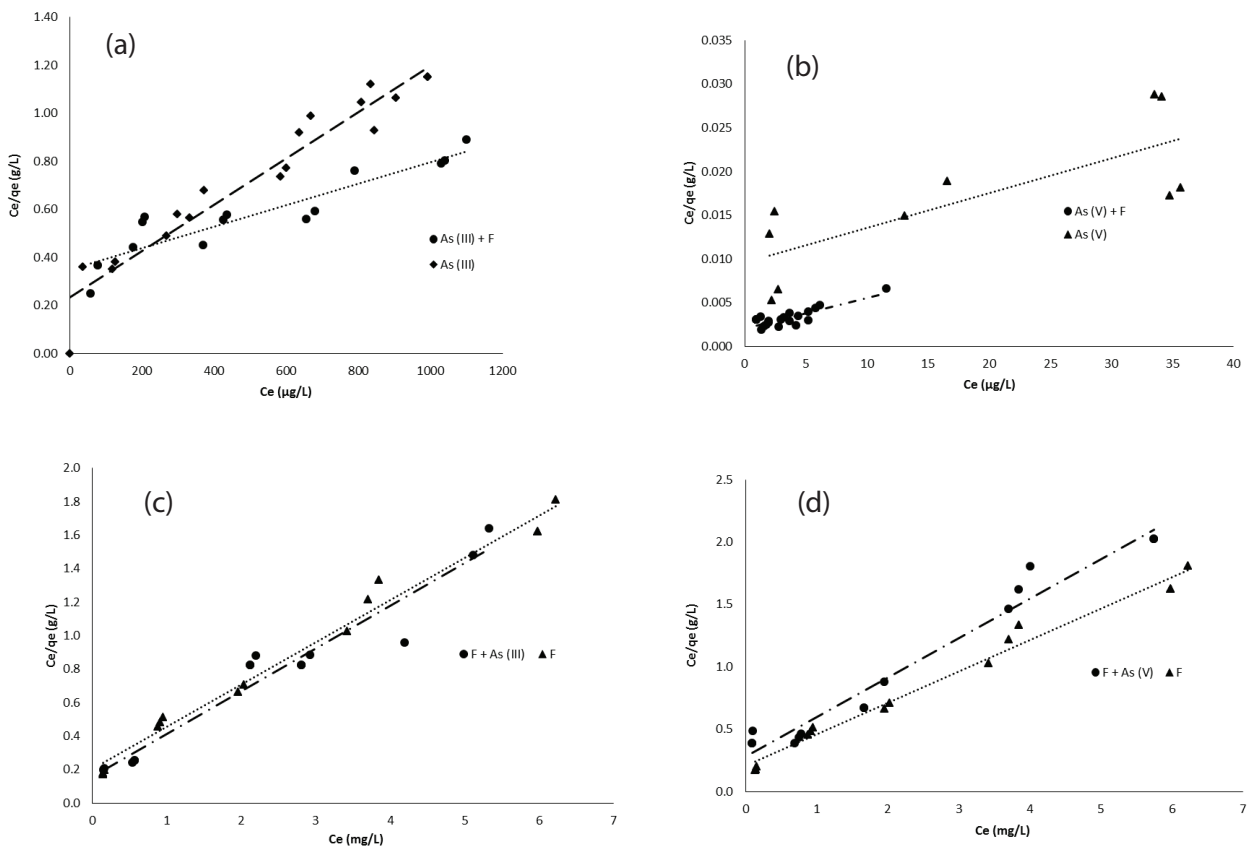


Fig. 8. Langmuir isotherm of (a) As(III), (b) As(V) adsorption onto iron oxide/alumina nanocomposites in the presence of fluoride (pH = 7.0, shaking speed = 180 rpm, temperature = 20°C). Langmuir isotherm of F adsorption onto iron oxide/alumina nanocomposites in the presence of (c) As(III) and (d) As(V) (pH = 7.0, shaking speed = 180 rpm, temperature = 20°C).

observed that the presence of F provided an antagonistic effect on As(V) removal by Al–Fe (hydr)oxides though the studies were carried out at higher initial concentrations of F (20 mg/L). The percentage removal of F in the presence of varying concentrations of As(III) and As(V) was also monitored and the results indicated that there was no significant change in percentage removal of F with increase in As concentration (Supplementary Figs. S1 and S2).

3.4.2.2. Fluoride adsorption in the presence of arsenic The presence of As(III) and As(V) provided a slight antagonistic effect towards F adsorption (Figs. 8(c) and (d)) and they followed the Langmuir isotherm model in both cases. In case of F adsorption in the presence of As(III), the q_m values were largely unaffected, decreasing to 3.85 mg/g from 4 mg/g in the presence and absence of As(III), respectively. In case of F adsorption in the presence of As(V), the q_m values decreased to 3.13 mg/g from 4 mg/g in the presence and absence of As(V), respectively. Qiao et al. [12] observed a 26% decrease in the F adsorption capacities of Al–Fe hydr(oxides) in the presence of arsenate. It was significant to observe that increase in F concentration led to a visible increase in the removal from 75% to 95% when the F concentration increased from 1 to 10 mg/L, respectively (Supplementary Fig. S3). The percentage removal of As(V) was unaffected by changes in F concentration with nearly 100% removal observed in all cases (Supplementary Fig. S4).

It is to be noted that the adsorption capacity of iron oxide/alumina nanocomposites presented here are based on the study with Millipore water. Groundwater has many ions such as sodium, magnesium, potassium, sulphate, calcium, nitrate, phosphate, chloride, etc [44]. Thus, the adsorption capacity would be different in the presence of other common groundwater ions. Depending on the type of ions (charge, molecular weight, solubility, etc) present, the capacity may possibly either increase, remain the same or even increase [45]. For example, the presence of phosphate in real groundwater samples was found to decrease fluoride adsorption (2% reduction) by iron nanoimpregnated particles [44]. On the other hand, the presence of Ca and Mg in groundwater

have been found to have synergistic effect on As(V) adsorption by TiO₂ nanoparticles due to electrostatic attraction, while exhibiting negligible effects towards As(III) [46].

To summarize, the presence of F, had a synergistic effect on As(III) and As(V) adsorption while a slight antagonistic effect was observed for F adsorption in the presence of As(III) and As(V). Table 3 provides a comparison of the adsorption capacity of several nanoadsorbents studied for arsenic and fluoride removal with the present study. It can be observed that most of the adsorbents have been used for the removal of a single contaminant. Factors such as pH, adsorbent dose, initial contaminant concentration, contact time, temperature, etc., play a significant role in determining the maximum adsorption capacity of an adsorbent in a system and are critically important when comparing adsorbents.

3.5. Adsorption kinetics

A study was also carried out to determine the kinetics of arsenic and fluoride adsorbed within the equilibration time. The change in As(III) and As(V) adsorbed within the equilibration time is shown in Fig. 9(a). The results obtained were in accordance with the As(III) and As(V) adsorbed at the end of 4 h. The adsorption of As(V) occurred more quickly and needed less time to reach equilibrium than that of As(III). Similarly, the 4 hour results of fluoride adsorbed from the short-term kinetics studies, as shown in Fig. 9(b), were in accordance with the results of the batch sorption study. The F adsorbed increased from 0.91 mg/g in 15 min to 1.72 mg/g in 4 h (Fig. 9(b)).

To further quantify the changes of arsenic and fluoride adsorption with time on iron oxide/alumina nanocomposites, pseudo-first-order and pseudo-second-order kinetic models were used to simulate the kinetics.

The pseudo-first-order reaction can be written as [47]:

$$\log(q_e - q_t) = \log q_e - \left(\frac{k_1}{2.303}\right)t \quad (6)$$

while the pseudo-second-order reaction can be written as [48]:

Table 3

Comparison of the sorption capacity of some adsorbents against As and F with iron oxide/alumina nanocomposites synthesized in this study

Nanoparticles	Contaminant	Adsorption capacity (mg/g)	Remarks	Reference
MgO	F	21.1	pH 5	[54]
Fe–Al–Ce	F	2.22	pH 7, initial F concentration 10 mg/L	[55]
SO ₄ -doped Fe ₃ O ₄ /Al ₂ O ₃	F	70.4	pH 7	[23]
Iron nanoimpregnated adsorbent	F	2.18	pH 7, adsorbent dose 2.5 g/L	[44]
MgO	As(V)	18.65	pH 7, adsorbent dose 1 g/L	[56]
Iron oxide	As, F	0.91 As(III) 3.33 As(V) 1.47 F	pH 7, adsorbent dose 1 g/L	[16]
Iron oxide/alumina nanocomposites	As, F	1.14 As(III) 2.5 As(V) 4 F	pH 7, adsorbent dose 1 g/L	This study

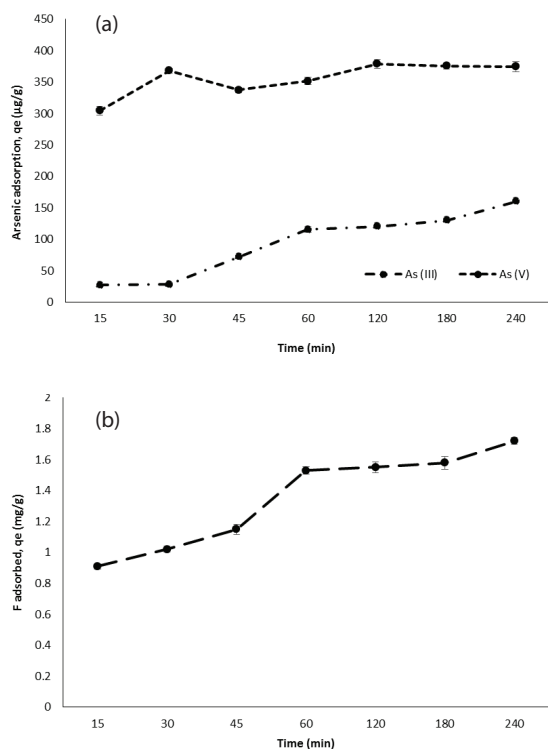


Fig. 9. (a) Short-term kinetics of arsenic adsorption as a function of time (pH = 7.0, concentration = 350 µg/L, shaking speed = 180 rpm, temperature = 20°C). (b) Short-term kinetics of fluoride adsorption as a function of time (pH = 7.0, concentration = 3 mg/L, shaking speed = 180 rpm, temperature = 20°C).

$$\frac{1}{(q_e - q_t)} = \left(\frac{1}{q_e} \right) + k_2 t \quad (7)$$

where q_e and q_t are the fluoride and arsenic adsorbed at equilibrium and at time t and k_1 and k_2 are the rate constants of the pseudo-first-order and pseudo-second-order reaction, respectively.

In all cases, the pseudo-second-order parameters better fitted with the data than the first-order parameters. The rate constant k_2 values of 0.0002, 0.007 and 0.038 were calculated for As(III), As(V) and F, respectively. The values of k_2 for As(V) adsorption were higher than those for As(III) adsorption under the same experimental conditions confirming that the removal of As(V) by iron oxide/alumina nanocomposites was faster than As(III). Table 4 summarizes the calculated parameters fitting the pseudo-first-order and pseudo-second-order reactions.

3.6. Antibacterial studies

Water is a source of several waterborne diseases with diarrhoea being the most common infectious waterborne disease in the developing world [49]. We attempted to develop an adsorbent which is effective against multiple inorganic contaminants with significant antibacterial activity against pathogenic microbes (though not the main focus of the paper). This would be the first significant step in enabling

Table 4

Summary of pseudo-first-order and pseudo-second-order reaction constants for arsenic and fluoride under optimized conditions (pH = 7; shaking speed = 180 rpm; temperature = 20°C; equilibration time = 4 h)

Type	k_1 (min)	R^2	k_2 (min)	R^2
As(III)	0.009	0.80	0.0002	0.89
As(V)	0.025	0.76	0.007	0.93
F	0.01	0.75	0.038	0.82

application of the nanoadsorbent in a point-of-use drinking water treatment system for effective removal of harmful contaminants.

Inorganic metal oxide nanoparticles have been determined to be effective disinfectants in view of their non-toxic profile, stability and antibacterial activities [50]. The antibacterial activity of iron oxide and alumina nanoparticles towards *E. coli* has been well documented. Iron oxide nanoparticles have been studied to cause the inactivation of *E. coli* by the diffusion of smaller particles into the membrane of the bacteria [51]. Another related study determined that there was a concentration dependant inhibition of *E. coli* on treatment with the iron oxide nanoparticles [52]. On the other hand, alumina nanoparticles have been observed to cause disruption of cell membrane and changes in the extracellular protein of *E. coli* [53]. In the present study, in order to determine the effectiveness of the synthesized nanocomposites against *E. coli*, the optical density was measured in nutrient broth, in the presence and absence of nanocomposites (Fig. 10(a)). Increase in the concentration of nanocomposites led to a corresponding inhibition in the growth of the bacterium. However, no complete inhibition of bacterial growth with time was observed at all the concentrations studied. A reduction in the optical density measured by ~60% was observed at the end of 24 h when a concentration of 4 mg/mL of nanocomposites was used as compared with control.

From Table 5, it was observed that an increase in the concentration of the nanocomposites led to a corresponding increase in the antibacterial activity. A 1 log reduction of *E. coli* was first observed at the end of 4 h when a concentration of 4 mg/mL nanocomposites was used. Further increase in the duration of treatment up to 24 h led to ~3 log reduction of bacteria. However, it was significant to observe that the nanocomposites were not as effective in inactivation of *E. coli* at the concentrations used for the arsenic and fluoride removal studies (1 mg/mL). A 1 log reduction of *E. coli* was observed after 24 h of treatment.

Increase in the duration of treatment led to an increase in the antibacterial rate (Fig. 10(b)). There was an increase in the antibacterial rate (%) with the corresponding increase in the concentration of nanocomposites. A 99.8% antibacterial rate was observed at the end of 24 h when a concentration of 4 mg/mL of nanocomposites was used.

The antibacterial studies revealed that the nanocomposites had significant activity against *E. coli* at higher concentrations with increase in duration of treatment. We could also observe that the nanocomposites were not effective as a disinfectant at the concentration studied for arsenic and fluoride removal studies.

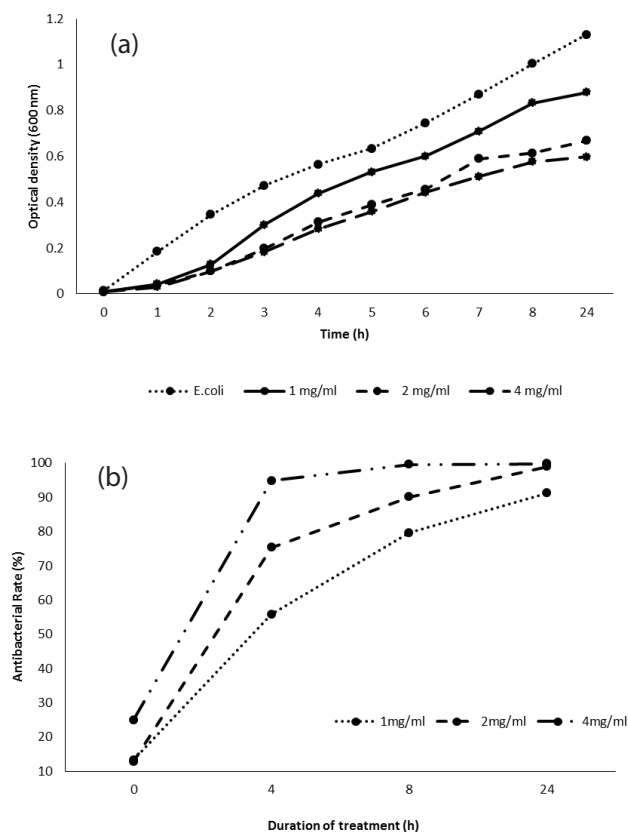


Fig. 10. (a) Growth curve of *E. coli* in the presence of different concentrations of nanocomposites (shaking speed = 180 rpm, temperature = 37°C). (b) Antibacterial rate (%) of nanocomposites (shaking speed = 180 rpm, temperature = 37°C).

Table 5

Antibacterial activity of different concentrations of iron oxide/alumina nanocomposites on *E. coli* (shaking speed = 180 rpm, temperature = 37°C)

	Log removal after different contact times			
	No. of bacteria/CFU at 0 h	4 h	8 h	24 h
Control	2.56×10^9	–	–	–
1 mg/mL	2.22×10^9	0.35	0.69	1.06
2 mg/mL	2.23×10^9	0.61	1	1.97
4 mg/mL	1.92×10^9	1.29	2.39	2.81

4. Conclusions

The present study demonstrated the application of iron oxide/alumina nanocomposites for the simultaneous removal of arsenic and fluoride from aqueous solutions. Stable nanocomposites with an average particle size of ~230 nm were obtained as evidenced by particle size analysis and SEM. The nanocomposites (at a concentration of 1 g/L) had significant adsorption efficiency for As(III) (~75%), As(V) (~99%) and F (~85%) at pH 7 and As concentration of 1,000 µg/L and F concentration of 1 mg/L, respectively.

The nanocomposites followed the Langmuir isotherm model and the kinetic data fitted the pseudo-second-order reaction kinetics with k_2 values of 0.0002, 0.007 and 0.038 for As(III), As(V) and F, respectively. The presence of F in the model water had a synergistic effect towards As(III) and As(V) removal by nanocomposites whereas the presence of As did not have a significant effect towards F removal. The nanocomposites demonstrated significant antibacterial activity towards *E. coli* at higher concentrations (4 mg/mL) with ~3 log reduction at the end of 24 h.

Acknowledgements

The authors are thankful to Prof. Amitava Mukherjee (VIT University, Vellore, India) and Rajeev Mudakavi (Indian Institute of Science, Bangalore, India) for help with BET and XRD analyses and also acknowledge the support of IHE lab staff in conducting various analyses. This research was funded by the People Programme (Marie Curie Actions) of the European Union's Seventh Framework Programme (FP7/2007-2013) under REA grant agreement no PCOFUND-GA-2013-606838.

References

- [1] S. Ayoob, A.K. Gupta, V.T. Bhat, A conceptual overview on sustainable technologies for the defluoridation of drinking water, *Crit. Rev. Environ. Sci. Technol.*, 38 (2008) 401–470.
- [2] I.A. Hamza, L. Jurzik, A. Stang, K. Sure, K. Uberla, M. Wilhelm, Detection of human viruses in rivers of a densely-populated area in Germany using a virus adsorption elution method optimized for PCR analyses, *Water Res.*, 43 (2009) 2657–2668.
- [3] S.V. Jadhav, E. Bringas, G.D. Yadav, V.K. Rathod, I. Ortiz, K.V. Marathe, Arsenic and fluoride contaminated groundwaters: a review of current technologies for contaminants removal, *J. Environ. Manage.*, 162 (2015) 306–325.
- [4] United Nations, Transforming Our World: The 2030 Agenda for Sustainable Development, A/RES/70/1, 2015.
- [5] D. Venieri, A. Fraggadaki, M. Kostadima, E. Chatzisyneon, V. Binas, A. Zachopoulos, G. Kiriakidis, D. Mantzavinos, Solar light and metal-doped TiO₂ to eliminate water-transmitted bacterial pathogens: photocatalyst characterization and disinfection performance, *Appl. Catal., B*, 144–145 (2014) 93–101.
- [6] D.N. King, M.J. Donohue, S.J. Vesper, E.N. Villegas, M.W. Ware, M.E. Vogel, E.F. Furlong, D.W. Kolpin, S.T. Glassmeyer, S. Pfaller, Microbial pathogens in source and treated waters from drinking water treatment plants in the United States and implications for human health, *Sci. Total Environ.*, 562 (2016) 987–995.
- [7] A. Pruss-Ustun, J. Bartram, T. Clasen, J.M. Colford, O. Cumming, V. Curtis, S. Bonjour, A.D. Dangour, J. De France, L. Fewtrell, M.C. Freeman, Burden of disease from inadequate water, sanitation and hygiene in low- and middle-income settings: a retrospective analysis of data from 145 countries, *Trop. Med. Int. Health*, 19 (2014) 894–905.
- [8] X. Qu, P.J.J. Alvarez, Q. Li, Applications of nanotechnology in water and wastewater treatment, *Water Res.*, 47 (2013) 3931–3946.
- [9] T. Thompson, J. Fawell, S. Kunikane, D. Jackson, S. Appleyard, P. Callan, J. Bartram, P. Kingston, Chemical Safety of Drinking Water: Assessing Priorities for Risk Management, World Health Organization, Geneva, VII 2007, p. 142.
- [10] WHO Guidelines for Drinking Water Quality, World Health Organization, Vol. 1, 4th ed., 2011, p. 178.
- [11] M. Amini, K.C. Abbaspour, M. Berg, L. Winkel, S.J. Hug, E. Hoehn, H. Yang, C.A. Johnson, Statistical modeling of global geogenic arsenic contamination in groundwater, *Environ. Sci. Technol.*, 42 (2008) 3669–3675.

- [12] J. Qiao, Z. Cui, Y. Sun, Q. Hu, X. Guan, Simultaneous removal of arsenate and fluoride from water by Al-Fe hydr(oxides), *Front. Environ. Sci. Eng.*, 8 (2014) 169–179.
- [13] R. Liu, W. Gong, H. Lan, T. Yang, H. Liu, J. Qu, Simultaneous removal of arsenate and fluoride by iron and aluminium binary oxide: competitive adsorption effects, *Sep. Purif. Technol.*, 92 (2012) 100–105.
- [14] V. Kumar, N. Talreja, D. Deva, N. Sankaramakrishnan, A. Sharma, N. Verma, Development of bi-metal doped micro- and nano multi-functional polymeric adsorbents for the removal of fluoride and arsenic(V) from wastewater, *Desalination*, 282 (2011) 27–38.
- [15] Y. Ku, H.M. Chiou, The adsorption of fluoride ion from aqueous solution by activated alumina, *Water Air Soil Pollut.*, 133 (2002) 349–360.
- [16] T.C. Prathna, S.K. Sharma, M. Kennedy, Development of iron oxide nanoparticle adsorbents for arsenic and fluoride removal, *Desal. Wat. Treat.*, 67 (2017) 187–195.
- [17] V.K.K. Upadhyayula, S. Deng, M.C. Mitchell, G.B. Smith, Application of carbon nanotube technology for removal of contaminants in drinking water: a review, *Sci. Total Environ.*, 408 (2009) 1–13.
- [18] J.K. Patra, K.H. Baek, Green biosynthesis of magnetic iron oxide (Fe_3O_4) nanoparticles using the aqueous extracts of food processing wastes under photo catalysed condition and investigation of their antimicrobial and antioxidant activity, *J. Photochem. Photobiol., B*, 173 (2017) 291–300. DOI: <https://doi.org/10.1016/j.jphotobiol.2017.05.045>
- [19] P.A. Prashanth, R.S. Raveendra, R. HariKrishna, S. Ananda, N.P. Bhagya, B.M. Nagabhushana, K. Lingaraju, H.R. Naika, Synthesis, characterizations, antibacterial and photoluminescence studies of solution combustion-derived $\alpha\text{-Al}_2\text{O}_3$ nanoparticles, *J. Asian Ceram. Soc.*, 3 (2015) 345–351.
- [20] A. Amirsalari, S.F. Shayesteh, Effects of pH and calcination temperature on structural and optical properties of alumina nanoparticles, *Superlattices Microstruct.*, 82 (2015) 507–524.
- [21] E. Sahin, S.J. Musevi, A. Aslani, Antibacterial activity against *Escherichia coli* and characterization of ZnO and ZnO- Al_2O_3 mixed oxide nanoparticles, *Arabian J. Chem.*, 10 (2017) S230–S235.
- [22] G. Wang, W. Jin, A.M. Qasim, A. Gao, X. Peng, W. Li, H. Feng, P.K. Chu, Antibacterial effects of titanium embedded with silver nanoparticles based on electron transfer induced reactive oxygen species, *Biomaterials*, 124 (2017) 25–34.
- [23] L. Chai, Y. Wang, N. Zhao, W. Yang, X. You, Sulfate-doped $\text{Fe}_3\text{O}_4/\text{Al}_2\text{O}_3$ nanoparticles as a novel adsorbent for fluoride removal from drinking water, *Water Res.*, 47 (2013) 4040–4049.
- [24] J. Lian, J. Ma, X. Duan, T. Kim, H. Li, W. Zheng, One step ionothermal synthesis of $\gamma\text{-Al}_2\text{O}_3$ mesoporous nanoflakes at low temperature, *Chem. Commun.*, 46 (2010) 2650–2652.
- [25] K.S. Ranjith, P. Manivel, R.T. Rajendrakumar, T. Uyar, Multifunctional ZnO nanorod-reduced graphene oxide hybrids nanocomposites for effective water remediation: effective sunlight driven degradation of organic dyes and rapid heavy metal adsorption, *Chem. Eng. J.*, 325 (2017) 588–600.
- [26] J. Sun, Z. Zhang, J. Ji, M. Dou, F. Wang, Removal of Cr^{6+} from wastewater via adsorption with high specific surface area nitrogen doped hierarchical porous carbon derived from silkworm cocoon, *Appl. Surf. Sci.*, 405 (2017) 372–279.
- [27] Z. Guo, T. Pereira, O. Choi, Y. Wang, H.T. Hahn, Surface functionalized alumina nanoparticle filled polymeric nanocomposites with enhanced mechanical properties, *J. Mater. Chem.*, 16 (2006) 2800–2808.
- [28] U. Janosovits, G. Ziegler, U. Scharf, A. Wokaun, Structural characterization of intermediate species during synthesis of Al_2O_3 -aerogels, *J. Non-Cryst. Solids*, 210 (1997) 1–13.
- [29] D. Mishra, R. Arora, S. Lahiri, S.S. Amritphale, N. Chandra, Synthesis and characterization of iron oxide nanoparticles by solvothermal method, *Prot. Met. Phys. Chem. Surf.*, 50 (2014) 628–631.
- [30] M.R. Das, J.M. Borah, W. Kunz, B.W. Ninham, S. Mahiuddin, Ion specificity of the zeta potential of α alumina, and of the adsorption of p-hydroxybenzoate at the α alumina-water interface, *J. Colloid Interface Sci.*, 344 (2010) 482–491.
- [31] J. Wang, W. Xu, L. Chen, X. Huang, J. Liu, Preparation and evaluation of magnetic nanoparticles impregnated chitosan beads for arsenic removal from water, *Chem. Eng. J.*, 251 (2014) 25–34.
- [32] S. Dixit, J.G. Hering, Comparison of arsenic(V) and arsenic(III) sorption onto iron oxide minerals: implications for arsenic mobility, *Environ. Sci. Technol.*, 32 (2003) 4182–4189.
- [33] D. Mohan, C.U. Pittmann Jr., Arsenic removal from water/wastewater using adsorbents – a critical review, *J. Hazard. Mater.*, 142 (2007) 1–53.
- [34] C.H. Liu, Y.H. Chuang, T.Y. Chen, Y. Tian, H. Li, M.K. Wang, W. Zhang, Mechanism of arsenic adsorption on magnetite nanoparticles from water: thermodynamic and spectroscopic properties, *Environ. Sci. Technol.*, 49 (2015) 7726–7734.
- [35] V.K. Rathore, D.K. Dohare, P. Mondal, Competitive adsorption between arsenic and fluoride from binary mixture on chemically treated laterite, *J. Environ. Chem. Eng.*, 4 (2016) 2417–2430.
- [36] C. Han, H. Li, H. Pu, H. Yu, L. Deng, S. Huang, Y. Luo, Synthesis and characterization of mesoporous alumina and their performances for removing arsenic(V), *Chem. Eng. J.*, 217 (2013) 1–9.
- [37] J. Mendoza-Barron, A. Jacobo-Azuara, R. Levya-Ramos, S. Berber-Mendoza, R.M. Guerrero-Coronado, L. Fuentes-Rubio, J.M. Martinez-Rosales, Adsorption of arsenic (V) from a water solution onto a surfactant-modified zeolite, *Adsorption*, 17 (2011) 489–496.
- [38] I. Langmuir, The constitution and fundamental properties of solid and liquids. Part I. Solids, *J. Am. Chem. Soc.*, 38 (1916) 2221–2295.
- [39] H. Freundlich, Ueber die Adsorption in Losungen, *Z. Phys. Chem.*, 57 (1906) 385–470.
- [40] C. Escudero, N. Fiol, I. Villaescusa, J.C. Bollinger, Arsenic removal by a waste metal (hydr)oxide entrapped into calcium alginate beads, *J. Hazard. Mater.*, 164 (2009) 533–541.
- [41] W.H. Xu, J. Wang, L. Wang, G.P. Sheng, J.H. Liu, H.Q. Yu, X.J. Huang, Enhanced arsenic removal from water by hierarchically porous $\text{CeO}_2\text{-ZrO}_2$ nanospheres: role of surface and structure dependent properties, *J. Hazard. Mater.*, 260 (2013) 498–507.
- [42] S.X. Zhang, H.Y. Niu, Y.Q. Cai, X.L. Zhao, Y.L. Shi, Arsenite and arsenate adsorption on coprecipitated bimetal oxide magnetic nanomaterials: MnFe_2O_4 and CoFe_2O_4 , *Chem. Eng. J.*, 158 (2010) 599–607.
- [43] E.T. Kamga, N. Audebrand, A. Darchen, Effect of co-existing ions during the preparation of alumina by electrolysis with aluminium soluble electrodes: structure and defluorination activity of electro-synthesized adsorbents, *J. Hazard. Mater.*, 254–255 (2013) 125–133.
- [44] I. Ali, Z.A. AlOthman, M.M. Sanagi, Green synthesis of iron nano-impregnated adsorbent for fast removal of fluoride from water, *J. Mol. Liq.*, 211 (2015) 457–465.
- [45] L. Yan, S. Hu, C. Jing, Recent progress of arsenic adsorption on TiO_2 in the presence of coexisting ions: a review, *J. Environ. Sci.*, 49 (2016) 74–85.
- [46] J. Cui, J. Du, S. Yu, C. Jing, T. Chan, Groundwater arsenic removal using granular TiO_2 : integrated laboratory and field study, *Environ. Sci. Pollut. Res.*, 22 (2015) 8224–8234.
- [47] S. Lagergren, Zur theorie der sogenannten adsorption gelöster stoffe, *K. Sven. Vetensk. akad. Handl.*, 24 (1898) 1–39.
- [48] G. McKay, Y.S. Ho, Pseudo second order model for sorption processes, *Process Biochem.*, 34 (1999) 451–465.
- [49] T. Clasen, S. Boisson, P. Routray, B. Torondel, M. Bell, O. Cumming, J. Ensink, M. Freeman, M. Jenkins, M. Odagin, S. Ray, A. Sinha, M. Suar, W.P. Schmidt, Effectiveness of a rural sanitation programme on diarrhoea, soil transmitted helminth infection and child malnutrition in Odisha, India: a cluster randomised trial, *Lancet Global Health*, 2 (2014) 645–653.
- [50] T. Gordon, B. Perlstein, O. Houbara, I. Felner, E. Banin, S. Margel, Synthesis and characterization of zinc/iron oxide composite nanoparticles and their antibacterial properties, *Colloids Surf., A*, 374 (2011) 1–8.
- [51] C. Lee, J.Y. Kim, W.I. Lee, K.L. Nelson, J. Yoon, D.L. Sedlak, Bactericidal effect of zero valent iron nanoparticles on *Escherichia coli*, *Environ. Sci. Technol.*, 42 (2008) 4927–4933.

- [52] E.N. Taylor, T.J. Webster, The use of super paramagnetic nanoparticles for prosthetic biofilm, *Int. J. Nanomed.*, 4 (2009) 145–152.
- [53] I.M. Sadiq, B. Chowdhury, N. Chandrasekaran, A. Mukherjee, Antimicrobial sensitivity of *Escherichia coli* to alumina nanoparticles, *Nanomed. Nanotechnol. Biol. Med.*, 5 (2009) 282–286.
- [54] N.A. Oladoja, S. Hu, J.E. Drewes, B. Helmreich, Insight into the defluoridation efficiency of nano magnesium oxide in groundwater system contaminated with hexavalent chromium and fluoride, *Sep. Purif. Technol.*, 162 (2016) 195–202.
- [55] L. Chen, H.X. Wu, T.J. Wang, Y. Jin, Y. Zhang, X.M. Dou, Granulation of Fe–Al–Ce nano-adsorbent for fluoride removal from drinking water by spray coating on sand in a fluidized bed, *Powder Technol.*, 193 (2009) 59–64.
- [56] K. Gupta, S. Bhattacharya, D. Chattopadhyay, A. Mukhopadhyay, H. Biswas, J. Dutta, U.C. Ghosh, Ceria associated manganese oxide nanoparticles: synthesis, characterization and arsenic(V) sorption behaviour, *Chem. Eng. J.*, 172 (2011) 219–229.

Supplementary materials

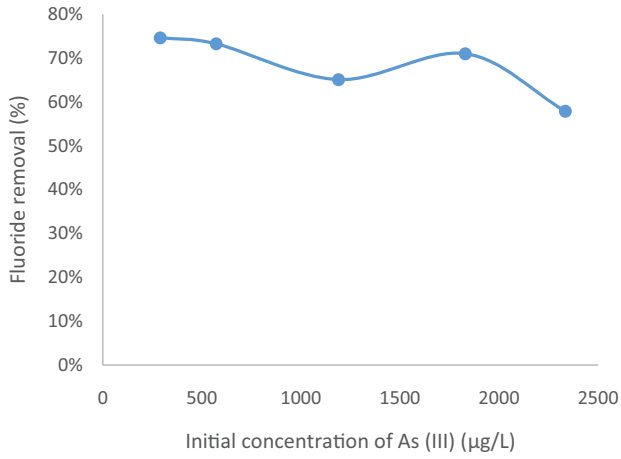


Fig. S1. Percentage removal of F in the presence of increasing concentrations of As(III).

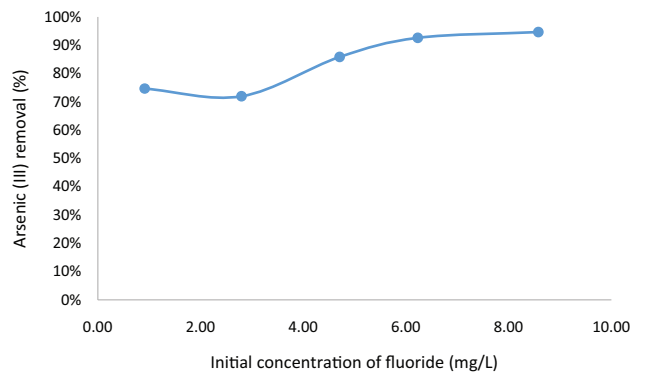


Fig. S3. Percentage removal of As(III) in the presence of increasing concentrations of F.

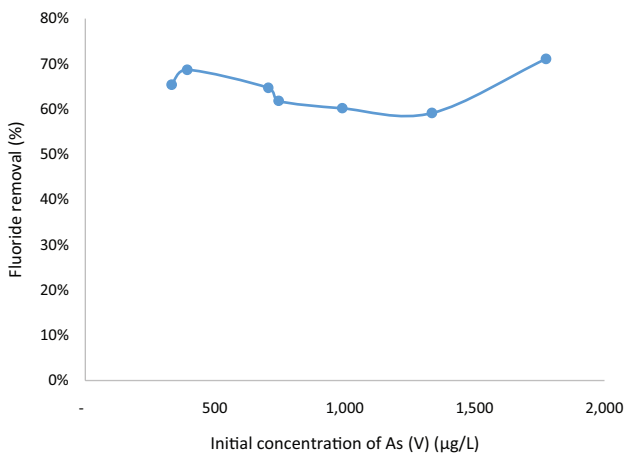


Fig. S2. Percentage removal of F in the presence of increasing concentrations of As(V).

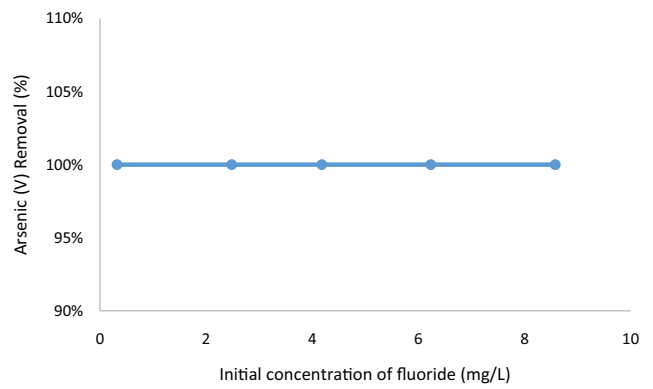


Fig. S4. Percentage removal of As(V) in the presence of increasing concentrations of F.